
Impact, Penetration, and Material Modeling

COPYRIGHTED MATERIAL

FRAGMENTATION OF CERAMICS IN THE BALLISTIC ENVIRONMENT

Dennis E. Grady

Applied Research Associates, Southwest Division, 4300 San Mateo Blvd NE
Albuquerque, New Mexico 87110, USA

ABSTRACT

The catastrophic disruption of materials in the ballistic environment commonly plays a central role in both the successful application of armor systems and the effective application of anti-armor systems. A theory of the dynamic fragmentation of solids based on continuum energy principles has provided a basis for assessing fragmentation in a wide range of ballistic applications over the past several decades^{1,2}. Applications of the theory to the fragmentation of brittle solids, including glass and ceramic, have been problematic, however. Recently, some of the physics issues governing length scales and size distributions in the dynamic fragmentation of brittle solids have come to light. The earlier energy-based fragmentation theory has been broadened to accommodate dynamic fragmentation in brittle materials. The paper summarizes past theories and their applications to fragmentation in the ballistic environment. More recent applications to ballistic fragmentation of glass and ceramic materials are described.

INTRODUCTION

Fragmentation of the component materials is a natural consequence of a terminal ballistic event. Commonly, the size distribution and trajectory of the resulting fragment debris is central to the effective application of the projectile or armor component specific to the event.

The multiplicity of materials of interest in terminal ballistic applications spans a wide range of breakup and fragmentation phenomena. The catastrophic fragmentation of brittle solids under the intense dynamic loading of the ballistic event is particularly interesting, and is perhaps the least understood.

The focus of this paper is on the dynamic fragmentation of brittle solids with particular emphasis on ceramic and glass. A theory of dynamic fragmentation for brittle materials is proposed. This theory is not a model of fragmentation for any specific application. Rather, the theory draws on underlying physical principles that determine the functional forms of the analytic relations that describe the statistical fragment size distributions and the fragmentation size length scales.

More broadly, the paper provides background on the topic of dynamic fragmentation of solids. The breadth and the richness of the topic are emphasized. At the same time previous theoretical work is outlined that is necessary to the present theoretical progress to brittle solids. The seminal wartime contributions of Nevill Mott^{3,4} to the area of dynamic fragmentation, integral to the progress, are recognized.

MOTT FRAGMENTATION

In the study of the dynamic fragmentation of solids there are several historical threads that can be traced. For those concerned with the topics of terminal ballistics or exploding munitions the seminal wartime effort of Nevill Mott^{3,4} is the most relevant. Of the several early efforts at achieving a theoretical understanding of dynamic fragmentation, the work of Mott has the more solid physical basis. The fragmentation theory of Mott predicts the two key elements of the dynamic fragmentation event. Namely, the statistical distribution in fragment size, and the governing distribution length scale or, equivalently, the average fragment size.

A feature of Mott's seminal theoretical study of fragmentation that has become a part of the lore in representation of terminal ballistics or exploding munitions fragmentation is the fragment distribution Mott plot. The Mott plot is a representation of the fragment distribution of a specific fragmentation

event where the logarithm of the cumulative fragment number larger is graphed against the individual fragment mass, $\ln N = f(m)$. Often the data plot linear, or near linear, in this semi-logarithmic representation of the fragment size data. Some contend that the Mott plot more specifically implies log number versus some specific power of the fragment mass. Mott himself vacillated on this point and, in one of his later wartime reports, suggested that a linear dependence on the mass m is perhaps the most appropriate. In any case, a Mott plot is here defined as a semilog plot of cumulative N versus m . The fragment size data do not always plot linear, but this representation is an appropriate space for a clear display of a broad body of dynamic fragmentation data.

Mott was principally concerned with a theoretical description of fragmenting munitions and expended most of his efforts in describing the breakup of explosion-driven expanding cylindrical cases. The Mott plots for several such case fragmentation experiments performed on AerMet 100 steel cylinders⁵ are shown in Figure (1).

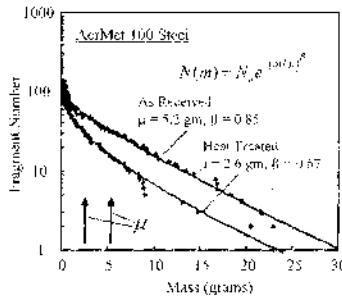


Figure 1. Mott fragmentation plots for two explosive tests on AerMet-100 steel cylinders.

Before embarking on the principal intent of this paper, there is value in observing some selected fragmentation data within the same Mott plot theme from more diverse areas of dynamic fragmentation.

An interesting counterpart to the exploding case fragmentation shown in Figure (1) occurs when a similar hollow cylindrical metal shell is instead imploded through placement of the explosive on the outside of the shell. Comparable kinetic energy imparted to the inward directed motion of the shell leads to intense shock compression and dissipation when the cylinder collapses towards the cylinder centerline. Shock dissipation is sufficiently intense that most of the metal either melts or is in a very hot solid state. The material motion is reversed when rebound at the centerline occurs. Fragmentation ensues with the hot liquid or solid metal particulating into fragments in the 10's to 100's of micrometer range. Ejected high-velocity fragments undergo subsequent aerothermal burning. Particle size distributions in such experiments have been determined by impeding witness plates⁶. A Mott fragmentation plot constructed from data from one test conveniently displays the fragment distribution as is shown in Figure (2).

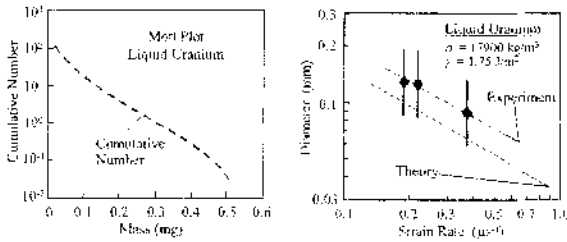


Figure 2. Mott plot for liquid fragments from one imploding metal cylinder fragmentation test is shown on the left. Fragment size data from witness plates and impact flux on one square centimeter. Mean fragment size versus expansion strain rate for three tests is displayed on the right⁶.

A starkly different dynamic fragmentation event is illustrated by the Hubble photograph in Figure (3) of fragmentation of the Shoemaker-Levi comet. Fragmentation is caused by gravitational forces as the comet passes the Roche limit on its downward trajectory towards the planet Jupiter. Fragment luminosity provides an approximate relative measure of the fragment masses. The fragment distribution Mott plot constructed for the comet fragments is shown in Figure (3).

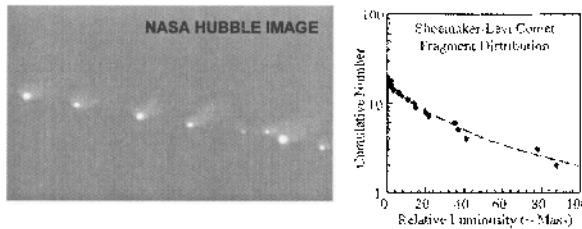


Figure 3. Hubble image of the fragmented Shoemaker-Levi comet and the fragment size Mott plot assessed from relative luminosity of comet fragments.

Spiraling down many decades in length scale, the process of nuclear spallation entails the relative high energy impact of atomic nuclei, resulting in a distribution of nuclear fragments. The experimental consequences of a carbon nucleus (atomic mass 12) onto a silver nucleus (atomic mass 107) nuclear spallation event⁷ are illustrated in Figure (4). Sixteen electrically charged fragments are produced ranging from deuterium (two nucleons) to beryllium (nine nucleons). A Mott plot of the data provides a sensible representation of the nuclear fragment distribution. The fragment distribution is reasonably represented by a simple exponential function⁸.

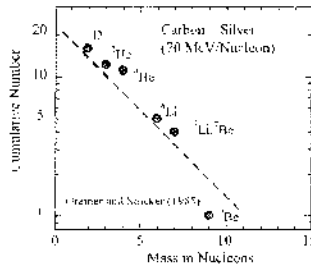


Figure 4. Fragmentation recorded in a photographic emulsion caused by the 70 MeV per nucleon collision of a carbon and a silver nucleus⁷. Cumulative fragment number distribution Mott plot constructed from the resulting nuclear fragment data⁸.

BRITTLE FRAGMENTATION

The selected examples of dynamic fragmentation in the previous section differ markedly in properties of the materials, the nature of the fragmentation, and the vast span of length scales separating the events. Yet, they exhibit some striking commonalities, and all are sensibly displayed in the Mott plot representation of the distribution data, or, a plot of log cumulative number versus fragment mass.

There are examples, however, of dynamic fragmentation where a Mott plot representation is not appropriate. Fragmentation of highly brittle materials, and perhaps other materials, results in fragment distributions that are poorly displayed on a Mott plot. Fragment fines are so numerous that counting fragments is not reasonable. Sieving techniques are used to separate fragments into size ranges. Fragment distributions are most commonly represented through plots of cumulative mass versus fragment size. Such distributions are observed to plot linear or near linear in a log cumulative mass versus log size display, or Schulmann distribution⁹, of the fragment size data. There are many examples of fragmentation of brittle materials that would make the salient points. An example is chosen here because of direct relevance to the terminal ballistics effects of interest.

The example is that of tests in which plates of boron carbide and composite are subjected to normal impact by tungsten carbide core armor piercing projectiles. Of interest here is the shatter fragmentation of the boron carbide ceramic. The authors of this study¹⁰ collected and determined size distributions for the resulting boron carbide fragment debris. Fragment distributions plotted in the Schulmann form⁹ are constructed from the data and are shown in Figure (5) from tests for several impact velocities. The near linear plots with power of order unity are representative of the behavior of brittle materials. Broadly, the power n ranges over about $0.5 < n < 1.5$, and occasionally higher, in Schulmann plots of brittle fragment distribution data.

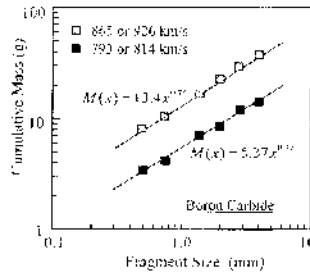


Figure 5. Schumann fragment size distribution plot constructed from data for boron carbide ceramic subjected to ballistic impact by tungsten carbide core projectiles¹⁰.

EQUILIBRIUM FRAGMENTATION

Before assessing the physics of fracture and fragmentation of brittle solids, it is necessary to first describe a theory of dynamic fragmentation that has demonstrated reasonably success for other materials. A representative set of test data that will be applied in describing this theory is shown in Figure (6). In these test the behind target fragment debris was captured and analyzed. The fragment size distribution Mott plots are shown for two tests from a series of experiments in which plates of stainless steel were subjected to impact by copper spheres over a selected range of impact velocities and angles of obliquity¹¹.

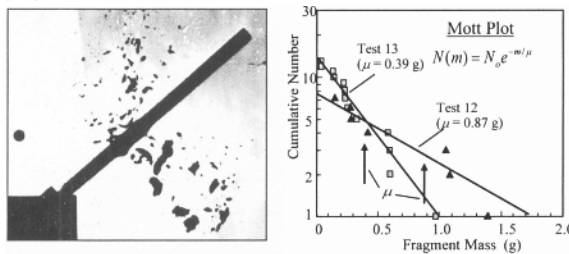


Figure 6. Impact of a copper spheres onto a stainless steel plates¹¹. Mott plot of the behind target fragment distribution for two such tests. Impact angle from normal and velocity: Test 12, 60 degrees, 3.26 km/s; Test 13, 50 degrees, 3.09 km/s.

As the fragmentation theory is described, reference will be made to equilibrium and nonequilibrium fragmentation. Briefly, equilibrium or nonequilibrium refers to the ability, or lack thereof, of the material to undergo fracture failure and fragmentation when a theoretical energy criterion is achieved. An energy criterion identifies onset of equilibrium fragmentation. Delayed failure and an additional failure criterion exemplify nonequilibrium fragmentation. At the present state of understanding equilibrium fragmentation appears to have fairly broad application across a range of material types. Nonequilibrium fragmentation applies to the brittle materials such as the competent ceramics and glasses. Some form of continuous transition from equilibrium to nonequilibrium fragmentation seems reasonable, however the boundaries of departure from one to the other are still poorly understood.

The fragment size distribution data for the two tests shown in Figure (6) are sensibly described by a

simple exponential function of the form,

$$N(m) = N_0 e^{-m/\mu} \tag{1}$$

The fragment size scale factor μ is observed to decrease as the intensity of the impact increases. In other words, higher velocity impacts resulting in more, but smaller, fragments.

The theory, and sought for physical understanding, is focused on two key elements; first, prediction of the distribution of fragment size resulting from the event, second, prediction of the distribution size scale μ and its dependence on the impact intensity and material properties.

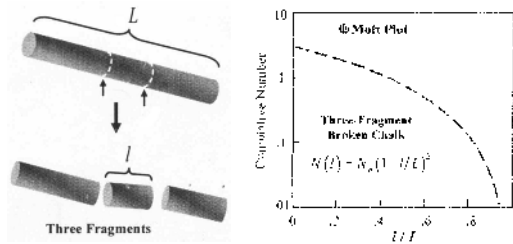


Figure 7. Length L is broken into three fragments with equal likelihood of fracture placement. The fragments size distribution Mott plot resulting from a binomial probability is shown on the right.

Fragment Size Distribution

I have heard a tale that if a stick of blackboard chalk (actually pressed gypsum in the later years of chalk and blackboard use) is dropped onto the floor, it breaks invariably into three pieces. (In today's increasing use of grease pencils and white boards this tale is rapidly becoming dated.) Whether true or not, it provides a theme for this first look at fragment size distributions. The chalk of length L in Figure (7) is broken at two places that are assumed to have equal likelihood of occurrence at any point within the length. The distribution of possible fragment sizes is governed by binomial statistics and yields the cumulative probability distribution for fragments of length l of the form^{8,12},

$$F(l) = 1 - (1 - l/L)^2 \tag{2}$$

The corresponding Mott distribution ($N_0 = 3$) is shown in Figure (7). If the number n of fragments that the length L is partitioned into is increased, the curve in the Mott plot becomes increasingly linear and in the limit the fragment distribution approaches the exponential form,

$$N(l) = N_0 e^{-l/\lambda} \tag{3}$$

where $\lambda = L/n$ is the average fragment length. Equation (3) is derived directly if an unbounded length is fractured along the length with frequency λ , in which case the fragment size distribution is determined from Poisson probabilities.

The present one-dimensional model results in an exponential distribution in fragment sizes not unlike the experimental results provided in Figure (6). One is encouraged to explore the random geometric fragmentation problem in two, and perhaps three, dimensions. Investigation of random geometric fragmentation and its possible application to real fragmentation has been undertaken by

various early workers in the field. One approach was pursued by Mott and Linfoot¹² in their initial report on munitions fragmentation. Some of this history is provided in a recent review¹⁴.

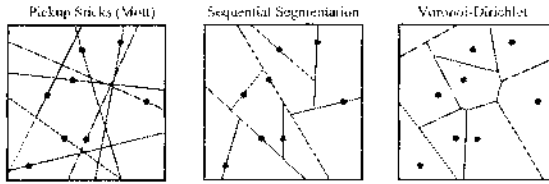


Figure 8. Three algorithms for randomly fragmenting a surface.

Consider random fragmentation in two dimensions. One immediately confronts a problem not evident in the random fragmentation of a line. Namely, a decision is necessary as to what form of algorithm to use in randomly partitioning the surface. Three of many possibilities are illustrated in Figure (8). Each algorithm starts through random placement of points on the surface. In the first, lines are scribed through the surface with random orientation. This fragmentation algorithm was investigated by Mott and Linfoot¹³ in some detail. For obvious reasons the algorithm has been identified as pick-up sticks fragmentation. In the second algorithm randomly oriented lines are sequentially scribed through the points that bisect the entered fragment. Third is the well-known Voronoi tessellation. Analytic expressions for the fragment size (area) distributions have been determined for each of the fragmentation algorithms, although some intuitive license is applied in one instance¹⁴. The pick-up sticks algorithm results in a Bessel function distribution of the fragment sizes. Sequential segmentation is exactly described by a simple exponential. The Voronoi tessellation provides a gamma function fragment size distribution. The Mott curves for each of the algorithms are compared in Figure (9).

Notably, much of the distribution for the three algorithms is nominally the same. It is only for a reasonably small fraction of the total at the small fragment tail of the distribution that the curves differ. The Voronoi algorithm results in a dearth of small fragments whereas the pick-up sticks algorithm leads to an excess.

One can speculate, based on the three examples that random geometric fragmentation of a surface, and by extrapolation a volume, will result in an exponential functional form with a single size scale parameter, although not necessarily a simple exponential. Further, the distribution is reasonable insensitive to the fragmentation algorithm (discounting the small fragment tail).

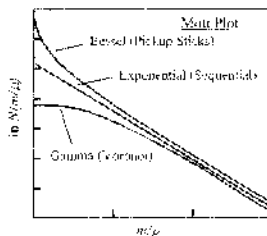


Figure 9. Fragment size distributions in Mott plot representation for three fragmentation algorithms.

The cumulative probability distribution for each of these examples can be written,

$$F(m) = 1 - e^{-h(m/\mu)} \quad (4)$$

where the likelihood function $h(m/\mu)$ will differ for each of the examples. The key point is that each of the distributions is constrained by a single length (size) scale μ which provides the scale factor for the distribution.

The preceding efforts have, of course, been an exercise in geometric fragmentation where a Poisson point process followed by a partitioning algorithm is used to randomly fragment a body. The dynamic fragmentation of many materials does not markedly differ from this geometric process, however. Dynamic spall in metals, for example, as exhibited by the images provided in the reviews of Shockey et al.¹⁵ and Curran et al.¹⁶, are processes in which fractures activate at random at independent points in the body, accelerate, grow, and ultimately coalesce to provided surfaces of the fragmented material. Physics-based models with increasing degrees of sophistication governing random fracture activation, growth and coalescence result in fragment distributions of the form provided in Equation (4).

The classic physics-based fragmentation model of Mott⁴ is a one-dimensional analysis undertaken to determine the distribution in spacings resulting from the axial splitting of explosively expanding munitions. The resulting distribution is of the form of Equation (4) with a power-law likelihood function $h(m) = (m/\mu)^\beta$. In the Mott model and analysis the resulting size scale is shown to be approximately $\mu \sim \sqrt{\rho Y / \rho \dot{\epsilon}}$, while the power is about $\beta \sim 7/2$. The material density and yield stress are ρ and Y , respectively, $\dot{\epsilon}$ is the strain rate of the expanding munitions, while γ is the Mott statistical fracture parameter^{4,12}.

These theoretical arguments, although not definitive, support the exponential or near exponential character observed in many of the dynamic fragment events where a single size scale parameter ties the distribution to the intensity of the event. Remaining then, is an assessment based on theoretical considerations of this size scale factor for a given dynamic fragmentation event.

Fragment Size Scale Factor

Again, the impact fragmentation experiment depicted in Figure (6) will provide the application for a theoretical assessment of the scale factor constraining the experimental fragment size distribution. Impact causes the dynamic fragmentation of a portion of the plate neighboring the point of impact. The fragment debris is ejected and expands with an intensity that is proportional to the impact velocity. If the impact velocity is increased the number of fragments produced is greater and the average fragment size is smaller. The scale factor μ in the exponential expression for the fragment size distribution accounts for the dependence on intensity of the fragmentation event.

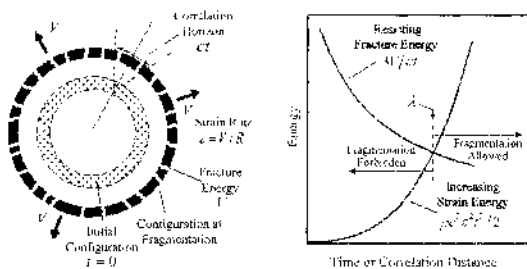


Figure 10. Model for visualizing the energies governing the characteristic fragment size in an equilibrium fragmentation event.

The principle issues concerning the fragmentation process in this example are captured in the idealized, but conceptually more transparent, model illustrated in Figure (10). A thin circular ring, or a spherical shell, of material is provided an initial impulse leading to asymmetrically outward expansion at a velocity V . (Deceleration due to deformation dissipation of the initial kinetic energy is ignored.) A sensible measure of the expansion intensity is provided by the expansion rate $\dot{\epsilon} = V/R$, where R is the radius of the ring or shell. If material deformation response to the imparted motion is linear elastic, then elastic strain energy increases with time according to,

$$U_s = \rho c^2 \dot{\epsilon}^2 t^2 / 2, \tag{5}$$

where c is an appropriate elastic wave speed that determines the elastic modulus of the material. After onset of expansion this wave speed also determines a correlation horizon². This correlation horizon determines at any time t a region of the material in which material points are within an elastic communication distance. Within the correlation horizon elastic stresses can adjust to modest variations in elastic modulus and concentrate stresses at points of weakness. A fundamental, and logically reasonable, precept of the theory is that, if fragmentation occurs within a time t , then fragments can be no larger than the region determined by the correlation horizon ct . A straightforward calculation provides a lower-bound fracture surface energy density over the body of,

$$U_f = 3\Gamma/ct, \tag{6}$$

where Γ is the fracture surface energy per unit area generated in the event. For example, if the body is a metal with fracture toughness K_I , then a reasonable estimate of the fracture energy is provided by $\Gamma \sim K_I^2/2\rho c^2$.

A plot of both the elastic strain energy in Equation (5) that will fuel the fracture process, and the resisting fracture energy in Equation (6) that will be supplied by the strain energy, are plotted as a function of the correlation distance (or time) on the right of Figure (10). The correlation horizon as the body expands is also illustrated in the picture on the left. The strain energy is for this example an increasing quadratic function of time. The resisting fracture energy required to fragment the body is correspondingly a decreasing function of time. Fragmentation is not allowed until the energies are equal. Equality occurs at a correlation distance identified as λ in the figure. Although certainly not required, an assumption of the present energy-based theory is that equilibrium fragmentation occurs when the two energies are nominally equal and the correlation length λ provides the scale factor constraining the fragment size distribution. For the exponential distributions describing the fragment

size data in Figure (6) the mass scale is $m \sim \rho \lambda^3$.

By equating the energy relations provided in Equation (5) and (6), an analytic expression,

$$\lambda = \left(\frac{6\Gamma}{\rho \dot{\epsilon}^2} \right)^{1/3}, \tag{7}$$

for the governing fragment size length scale is directly calculated from both fracture properties of the material and a strain rate measure of the intensity of the fragmentation event. Application of Equation (7) to the tests provided in Figure (6) based on properties for stainless steel and kinematic properties of the fragmentation event provide size scale factors that are in remarkably good agreement with the experimental results. Similar successes of the theory have been demonstrated in numerous other applications in dynamic fragmentation¹⁴.

NONEQUILIBRIUM (BRITTLE) FRAGMENTATION

Nonequilibrium fragmentation, in contrast to equilibrium fragmentation, occurs in those materials that, when subjected to dynamic fragmentation conditions appropriate to the plot in Figure (10), do not fail at the juncture of the two energy curves. Instead, elastic strain energy continues to increase until some other failure criterion is achieved. In the present context this behavior applies to glass and to certain very competent ceramics such as boron carbide. As noted earlier, nonequilibrium fragmentation most probably occurs to some extent in numerous other materials. This interpretation of the energy-based fragmentation theory is less mature and has not yet been extensively explored^{14,17}.

Theoretical Basis

The comparable energy plot for nonequilibrium fragmentation is illustrated in Figure (11). When strain energy is achieved that is necessary to fuel the required fracture energy, all conditions sufficient for failure and fragmentation are not present. Strain energy, correlation length, and time continue to increase until an alternative criterion is achieved that provides both the necessary and the sufficient conditions for failure.

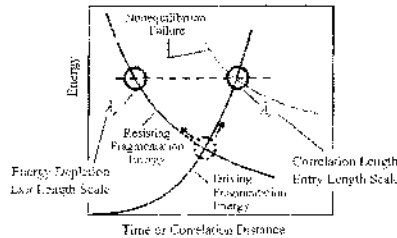


Figure 11. Nonequilibrium conditions leading to a schism in length scales spanning the fragment size distribution in brittle solids.

An application of nonequilibrium fragmentation perhaps most easily visualized is that of spall in glass. In the spall process release waves interact and carry regions of the glass into tension at a high rate of strain (of order 10⁷/s to 10⁹/s). Because of the very modest energy required to create new fracture surface in glass, strain energy necessary for failure and fragmentation occurs at a tension of a few tenths of a GPa. Experimental studies show, however, that tensile stresses in the neighborhood of several GPa (one order of magnitude higher) are achieved before the spallation of glass. Reasons for the markedly high spall strengths of glass presumably relate to the very modest defect structure in the

material, and the stress and stress correlation states that must be achieved to activate internal cavitation.

Although more complex, similar nonequilibrium fragmentation governs failure in the ballistic impact tests on boron carbide ceramic target plates for which the fragment size distribution data are shown in the previous Figure (5). Namely, elastic strain energy achieves levels that far exceed the required fracture energy before failure and fragmentation proceeds. Again, the material defect structure, joined with the elastic strain energy and strain energy history, combine to determine the elevated nonequilibrium state at which failure begins.

The correlation length scale λ_c at onset of failure determines the initial fabric of fracture. Fractures on a spacing of this characteristic length scale, however, are not sufficient to dissipate the excess elastic strain energy stored in the body preceding failure. Fracture failure proceeds through successive crack branching until available strain energy is exhausted and a fracture fabric is achieved commensurate with the fracture surface energy length scale λ_s identified in Figure (11).

In summarizing to this point, certain competent brittle solids do not exhibit equilibrium fragmentation governed by a single length scale λ occurring at the juncture of the elastic strain energy and fracture resistance energy curves as shown in Figure (10). Such brittle solids instead exhibit nonequilibrium fragmentation governed by an alternative, markedly higher energy, failure criterion that leads to a schism in length scales as illustrated in Figure (11). The correlation length scale λ_c and surface energy length scale λ_s can be decades apart in highly nonequilibrium dynamic fragmentation applications.

Much of the dynamic fracture and fragmentation physics is enveloped by the surface fracture energy and correlation length scales λ_s and λ_c . Onset of failure and initial fracture is governed by the correlation length scale λ_c . Continued fracture, through successive crack branching, cascades down through the length scales until strain energy is exhausted at the length scale λ_s . Over a range of length scales bounded by λ_s and λ_c , the physics of fracture is independent of length scale. Physical processes become self-similar within this range and physical symmetry dictates that such processes are described by power-law functions of the length scale $\lambda_s < x < \lambda_c$. The general concepts have application to other areas of physics including hydrodynamic turbulence¹⁶ and fatigue fracture¹⁹. This physics has been referred to as a *law of intermediate asymptotics*.

In particular, within this range of length scales the resulting distribution of fragment sizes is necessarily power-law. Expressed as a cumulative fragment number distribution greater than size x , the distribution is written in the form,

$$N(x) \sim x^{-d}, \quad (8)$$

where the exponent d is the fractal dimension of the distribution²⁰. The distribution is readily transformed to the Schuermann mass distribution,

$$M(x) = M_p x^n, \quad (9)$$

where the Schuermann index n is related to the fragment size fractal dimension²⁰ through $n = 3 - d$. A complete fragment distribution spanning the upper and lower length scales would, of course, be functionally more complex, but must be asymptotic to power-law behavior in the intermediate range.

The energy-based theory of nonequilibrium fragmentation provides a qualitative explanation for the ballistic impact generated fragment size distribution for boron carbide ceramic shown in Figure (5), as well as many other applications of dynamic fragmentation of brittle solids. The data are clearly described by a power-law function that span a finite range of fragment sizes. A more quantitative assessment of fragmentation requires both a clearer description of the impact conditions and a criterion for failure under the dynamic loading imposed.

Experimental Observations

The fragment distribution data from Figure (5) for ballistic impact tests on boron carbide ceramic¹⁶ are repeated in Figure (12) and compared with a qualitative description of the fragment distribution inferred from the theory. The character of the experimental fragment size distribution is in sensible agreement with the predicted theoretical behavior. The measured sieve data are consistent with a power-law distribution. It can be safely inferred that the experimental distribution exhibits an upper and lower bound.

A number of further questions, however, are raised concerning the theory. How are the correlation and energy length scales that determine the range of power-law behavior calculated? What is the appropriate dynamic failure criterion in the nonequilibrium fragmentation event? What properties of the material and/or the fragmentation event determine the exponent n in the power law? What is the span of the power-law range? Although not yet fully understood, these and related issues are discussed in the closing topics of this manuscript.

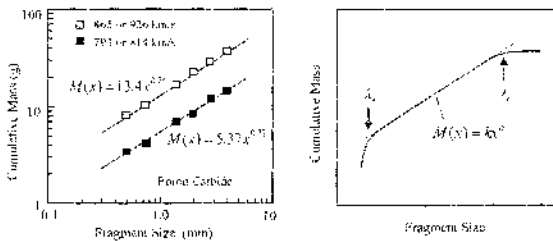


Figure 12. Experimental fragment size data for boron carbide ceramic¹⁶ and a qualitative comparison with the functional character of the nonequilibrium fragmentation theory.

Brittle Failure Criteria

Energy-based fragmentation of brittle solids under equilibrium conditions provides a failure criterion firmly founded on commonly available properties of the materials. Failure occurs at the juncture of the elastic strain energy and fracture energy curves shown in Figure (10), allowing direct calculation of the governing fragment size length scale as well as both the time and stress to failure under the loading conditions imposed.

Nonequilibrium fragmentation enters a realm in which the failure properties of brittle solids are not well understood. In the brittle solids of interest elastic strain energies under the loading conditions imposed achieve dynamic levels that far exceed equilibrium values before failure and subsequent fragmentation occurs. Failure activates at internal or surface sites of weakness under stress and time conditions that are poorly understood. A first-order assessment of the Figure (5) boron carbide experiments within the present fragmentation model is achieved by assuming that a nonequilibrium elastic strain energy commensurate with the Hugoniot elastic limit ($\sigma_{HE} \sim 15$ GPa) is attained within approximately one transit of the plate thickness before failure and fragmentation proceeds. These conditions would place the correlation length scale λ_c of the order of the plate thickness ($\lambda_c \sim 5$ mm). The lower energy length scale is calculated,

$$\lambda_c = 3(K_f / \sigma_{HE})^2 \tag{10}$$

and, with a reasonable fracture toughness of $K_f \sim 5$ MPa m^{1/2}, provides $\lambda_c \sim 0.3$ μ m. The two length scales clearly span the power-law distribution displayed in Figure (5).

Computational simulations of the time history of elastic strain accumulation in the impact event are readily performed. The span of power-law fragmentation would be provided through the theory if a credible failure criterion can be applied within the computational model.

A failure criterion that has achieved some success in the fracture of brittle solids, as well as other critical state phenomena, is that attributed to Tuler and Butcher²¹. The Tuler-Butcher failure criterion can be expressed in the integral form,

$$I_{TB} = \int (\sigma(t) - \sigma_m)^m dt \leq K_m. \quad (11)$$

The stress applicable to the applied loading conditions is σ , while σ_m is a corresponding threshold value of the stress. Failure occurs when the time-dependent Tuler-Butcher integral achieves the material constant K_m . The exponent m is a property of the material. For $m=1$, Equation (11) provides an impulse criterion, whereas for $m=2$ the same equation is an energy or work criterion. As m becomes large Equation (11) approaches a constant stress failure criterion. When fit to experimental data an exponent m close to two is frequently observed. Impact breach tests on plates of soda-lime glass of Sun et al.²², for example, are described by a Tuler-Butcher failure criterion with $m=2$ for the Tuler-Butcher index²³. The Tuler-Butcher criterion is appropriate for analytic models of ballistic failure where the stress within the integral is a sensible average over the elastic strain energy contribution to the catastrophic fragmentation²⁴. The Tuler-Butcher criterion also has application in computational simulation.

Fragmentation Intensity Number

In the theory of hydrodynamic turbulence the magnitude of the Reynolds number provides a measure of the extent of the inertial range – the span of length scales encompassing the entry level system scale powering the hydrodynamics, down to the limiting substructure scale necessary for the viscous dissipation. A similar dimensionless number characterizing the self-similar power-law range of the fragmentation event can be constructed by the ratio of the limiting correlation and energy length scale,

$$F = \lambda_c / \lambda_e. \quad (12)$$

If the kinematic state of the body leading to failure can be characterized by a single strain rate $\dot{\epsilon}$, then the limiting correlation length λ_c and the stress at failure of the body are related through,

$$\sigma = \rho c \dot{\epsilon} \lambda_c. \quad (13)$$

The energy limiting lower-bound length scale λ_e is related to the failure stress through,

$$\frac{\sigma^2}{2\rho c} = \frac{3\Gamma}{\lambda_e}, \quad (14)$$

where Γ is the fracture surface energy. Solving for $F = \lambda_c / \lambda_e$ yields,

$$F = \frac{\sigma^3}{6\Gamma\rho^2 c^2}. \quad (15)$$

In a complex body (a projectile impacting a brittle plate for example) σ provides a stress measure of the stored elastic strain energy at the onset of failure. For fragmentation intensity number F in the neighborhood of unity the stress can be solved for,

$$\sigma = (61 \rho^2 c^2 \dot{\epsilon})^{1/3}. \quad (16)$$

This is the failure stress under conditions of equilibrium fragmentation. The intensity number increases rapidly with stress as failure criteria in excess of equilibrium are achieved.

Correlation Horizon

The concept of a correlation horizon² and the meaning of this correlation within the present context of dynamic fragmentation is worthy of additional thought. Consider the thin-walled spherical shell of metal as representative of the model depicted in Figure (10). The model assumes abrupt impulsive loading up to a uniform outward velocity V . In principle this initial requirement is physically reasonable. A step pressure of magnitude $P = \rho c V$ could be applied uniformly over the inner surface of the shell. A shock would propagate through the thickness d of the shell, reflect from the free surface and return a release wave. If the step pressure is maintained for a time $2d/c$, the impulse conditions sought are achieved. (Elastic-plastic behavior is ignored in this discussion.)

As outward motion proceeds, a uniform circumferential tension increases with time; the stress underlying the strain energy of Equation (5). In a continuum first-order assessment this time-dependent tension is independent of position throughout the body. Stress correlation plays a role in all real materials in that the modulus of elasticity is a function of circumferential position about the shell. Any number of practical reasons can be responsible for this position dependence. The fluctuation with position would be quite subtle in a glass material for instance. It would be markedly more pronounced in other engineering materials. Thus, the correlation of circumferential stress is time dependent and determined by the elastic wave speed. A weakest point (in the sense of fracture activation) in the body within a given correlation horizon may not necessarily be the weakest point at a lower loading rate where the correlation horizon is correspondingly larger.

The necessity of a correlation distance, and a corresponding correlation time, is evident in the direct imaging of impact fracture and fragmentation experiments on glass and ceramic plates of Staussberger et al.²⁴. In those tests the failure-induced stress wave is observed to propagate radially outward from the point of impact well ahead of any observed onset of fracture damage. These data are a clear example of the need for time-dependent stress correlation and concentration at preferred sites in the body to bring about brittle fracture and fragmentation.

Power-Law Fragmentation

Fundamental physics demands that the fragment size distribution within the range of the two bounding length scales λ_1 and λ_2 , and sufficiently removed from either, be a power-law function of the fragment size. This physics is, of course, based on the proposed continuum fragmentation theory and the absence of any further intervening physical length scales. The same physics does not constrain the power-law exponent, however. Assessment of the exponent requires other physics be brought to bear.

The power-law nature of fragment size distributions resulting from the breakage of brittle solids has been noted by many since early in the last century, and probably earlier. Empirical evidence place the exponent n in the Schulmann relation $M(x) \sim x^n$ within the range of about $0.5 < n < 1.5$, with some applications achieving values approaching two and perhaps somewhat higher. There are studies in which values of n remarkably close to unity are observed²⁵. A number of the earlier studies invoked the random placement of fracture flaws (a Poisson process) and some random geometric partitioning of the body. Notable are the theoretical efforts of Gaudin²⁶, Bennett²⁷, Lienau²⁸ and Gilvart²⁹.

An intriguing alternative theoretical effort within this time frame was explored by Griffith³⁰. He

suggested an energy argument in which a specific energy $\alpha = \gamma/\rho x$ is associated with a fragment of size x . The fracture surface energy and specific density are γ and ρ , respectively. He then invoked classical statistical mechanics to arrive at a Boltzmann representation of the fragment size distribution. In the large fragment limit a power-law distribution with $n = 1$ is achieved. Arguments are also offered for distribution in which $n = 1$.

Turcott²⁰ has pursued the fragmentation of brittle solids as a fractal process leading to $N \sim x^{-d}$, or correspondingly to $M \sim x^a = x^{3-d}$, relating the exponent a to the fractal dimension d . Turcott explored group renormalization methods used by others to characterize various scale invariant critical state phenomena. He identifies a parameter p_w that determines the probability of fracturing of a cell of the solid body. The fractal dimension d is calculated from p_w , which he in turn relates to the fragility of the brittle material.

CONCLUSIONS

A theory of the dynamic fragmentation of solids based on continuum energy principles has provided a basis for assessing fragmentation in a wide range of ballistic applications over the past several decades. Applications of the theory to the fragmentation of brittle solids including glass and ceramic have been problematic, however. Recently, some of the physics issues governing length scales and sized distributions in the dynamic fragmentation of brittle solids have come to light. The earlier energy-based fragmentation theory is being broadened to accommodate dynamic fragmentation in brittle materials. The paper summarizes past theories and their applications to fragmentation in the ballistic environment. More recent applications to ballistic fragmentation in glass and ceramic materials are described.

The principal conclusion from this study is that a previous continuum energy-based fragmentation theory has application to both equilibrium (principally ductile materials) and nonequilibrium (brittle materials) fragmentation. The latter application, however, requires an additional failure criterion which is, at present, not well understood.

REFERENCES

- ¹D.E. Grady, Local Inertial Effects in Dynamic Fragmentation, *J. Appl. Phys.*, **53**, 322-325 (1982).
- ²D.E. Grady, The Spall Strength of Condensed Matter, *J. Mech. Phys. Solids*, **36**, 3, 353-384 (1988).
- ³N.F. Mott, A Theory of the Fragmentation of Shells and Bombs, *United Kingdom Ministry of Supply AC4035*, May (1943).
- ⁴N.F. Mott, Fragmentation of Shell Cases, *Proc. Royal Soc.*, **A189**, 300-308, January (1947).
- ⁵L. Chhabildas, W. Reinhart, L.T. Wilson, D.R. Reedal, D.E. Grady, J.W. Black, Fragmentation Properties of AerMet 100 Steel in Two Material Conditions, *Proceedings 19th International Symposium on Ballistics*, Interlaken, Switzerland, I.R. Crewther, ed., 663-670, May 7-11 (2001).
- ⁶D.E. Grady, Analysis of Prompt Fragmentation in Explosively-Loaded Uranium Cylindrical Shells, *Sandia National Laboratories Technical Report*, SAND82-0140, February (1982).
- ⁷W. Greiner and H. Stocker, *Sci. Am.* **252**, 76 (1985).
- ⁸D.E. Grady, Particle Size Statistics in Dynamic Fragmentation, *J. Appl. Phys.*, **68**, 12, 6099-6105 (1996).
- ⁹R. Schuhmann, Principles of Commiunition, I. Size Distribution and Surface Calculations, *AIIME Tech. Publ.* 1189, *Mining Technology*, 1-11 (1940).
- ¹⁰T.J. Moynihan, J.C. LaSavia, M.S. Burkins, Analysis of Shatter Gap Phenomenon in a Boron Carbide/Composite Laminate Armor System, *Proc. Int. Ballistics Symp.*, Sept. (2002).
- ¹¹D.E. Grady, C.A. Hall, W.D. Reinhart, *Sandia National Laboratories Technical Memorandum*, unpublished, (1996).
- ¹²D.E. Grady, *Fragmentation of Rings and Shells*, Springer, (2006).

- ¹³N.F. Mott and F.H. Linfoot, A Theory of Fragmentation, *United Kingdom Ministry of Supply* AC3348, February (1943).
- ¹⁴D.E. Grady, Dynamic Fragmentation of Solids, in *Shock Waves Science and Technology Reference Library* Vol. 3, Y. Horie, ed. (2009).
- ¹⁵D.A. Shockey, L. Seaman, D.R. Curran, in *Metallurgical Effects at High Strain Rates*, R.W. Rohde et al., eds., Plenum (1973).
- ¹⁶D.R. Curran, L. Seaman, D.A. Shockey, Dynamic Failure of Solids, *Physics Repts.*, **147**, 253-288 (1987).
- ¹⁷D.E. Grady, Fragment Size Distributions from the Dynamic Fragmentation of Brittle Solids, *Int. J. Impact Engng.*, **35**, 1557-1562 (2008).
- ¹⁸G. Falkovich and K.R. Sreenivasan, Lessons from Hydrodynamic Turbulence, *Physics Today*, **59**, 4, 43-49 (2006).
- ¹⁹G.I. Barenblatt, Scaling Phenomena in Fatigue and Fracture, *Int. J. Fracture*, **138**, 19-35 (2006).
- ²⁰D.L. Turcotte, Fractals and Fragmentation, *J. Geophys. Res.*, **91**, 1921-1926 (1986).
- ²¹F.R. Tuler and B.M. Butcher, A Criterion for the Time Dependence of Fracture, *Int. J. Fracture Mech.*, **4**, 431-437 (1968).
- ²²X.M. Sun, A. Khaleel, R.W. Davies, Modeling of Stone-Impact Resistance of Monolithic Glass Ply Using Continuum Damage Mechanics, *Int. J. Damage Mech.*, **14**, 165-178 (2006).
- ²³D.E. Grady, Analysis of Shock and High-Rate Data for Ceramics: Failure and Fragmentation in the Shock and Ballistic Environment, Prepared for, U.S. Army TACOM-TARDEC, *Applied Research Associates Tech. Rept.*, April (2008).
- ²⁴E. Straussberg, P. Parimal, J.W. McCauley, C. Kovatchick, K.T. Ramesh, D.W. Templeton, High-Speed Transmission Shadowgraphic and Dynamic Photoelasticity Study, *Army Research Laboratory Rept.*, AR1.-RP-203, March (2008).
- ²⁵H.C. Bergstrom, C.L. Sollenberger, W. Mitchell, Energy Aspects of Single Particle Crushing, *Trans. AIME*, **220**, 367-372 (1961).
- ²⁶A.M. Gaudin, Investigation of Crushing Phenomena, *AIME Trans.*, **73**, 253-316 (1926).
- ²⁷J.G. Bennett, Broken Coal, *J. Inst. Fuel*, **10**, 22-39 (1936).
- ²⁸C.C. Lienuu, Random Fracture of a Brittle Solid, *J. Franklin Inst.*, **221**, 485-494, 674-686, 769-787 (1936).
- ²⁹J. Gilvarry, Fracture of Brittle Solids. I. Distribution Function for Fragment Size in Single Fracture (Theoretical), *J. Appl. Phys.*, **32**, 391-399 (1961).
- ³⁰L. Griffith, A Theory of the Size Distribution of Particles in a Comminuted System, *Canadian Journal of Research*, **21A**, 6, 57-64 (1943).